Available online at www.sciencedirect.com
ScienceDirect
International Journal of Heat and Fluid Flow 28 (2007) 1518–1530
International Journal of HEAT AND FLUID FLOW
www.elsevier.com/locate/ijhff

Modeling fluid and heat transport in the reactive, porous bed of downdraft (biomass) gasifier

Avdhesh Kr. Sharma *

Deenbandhu C.R. University of Science and Technology, Murthal, Sonepat, Haryana 131039, India

Received 14 June 2006; received in revised form 25 December 2006; accepted 15 February 2007
Available online 5 April 2007

Abstract

A fluid flow and heat transfer model has been developed for the reactive, porous bed of the biomass gasifier to simulate pressure drop, temperature profile in the bed and flow rates. The conservation equations, momentum equation and energy equation are used to describe fluid and heat transport in porous gasifier bed. The model accounted for drag at wall, and the effect of radial as well as axial variation in bed porosity to predict pressure drop in bed. Heat transfer has been modeled using effective thermal conductivity approach. Model predictions are validated against the experiments, while effective thermal conductivity values are tested qualitatively using models available in literature. Parametric analysis has been carried out to investigate the effect of various parameters on bed temperature profile and pressure drop through the gasifier. The temperature profile is found to be very sensitive to gas flow rate, and heat generation in oxidation zone, while high bed temperature, gas flow rate and the reduction in feedstock particle size are found to cause a marked increase in pressure drop through the gasifier. The temperatures of the down stream zones are more sensitive to any change in heat generation in the bed as compared to upstream zone. Author recommends that the size of preheating zone may be extended up to pyrolysis zone in order to enhance preheating of input air, while thermal insulation should not be less than 15 cm.

Keywords: Modeling gasifier; Heat and fluid transport; Porous bed; Producer gas; Gasifier

1. Introduction

The flow of fluids through porous media is of great practical importance in many diverse applications, including the drying the wet biomass particles or grain seeds, the gasification of biomass or coal, ground water movement, regenerative heat exchange, surface catalysis of chemical reactions etc. In all these instances it is necessary to predict design parameters such as pressure drop, friction factor, heat transfer coefficients in order to predict optimum operating conditions, size and design of equipment. In the past there has been a steady effort to improve the knowledge in this area. In most cases, Darcian flow assumed; however, some researchers have concentrated into non-Darcian flow as well. The pressure gradient across the porous bed is a function of system geometry, medium porosity, permeability and physical properties of working medium. Considerable progress has been made in past in establishing the relationship among velocity versus pressure drop or Reynolds number versus friction factor.

Ergun (1952), Ranz (1952), Brownell et al. (1956), Tallmadge (1970), Comiti et al. (2000) developed dimensionless form to establish the relationship in frictional factor and Reynolds number to describe the fluid transport through porous media as

$$f_{\text{pore}} = \alpha/Re_{\text{pore}} + \beta/Re_{\text{pore}}^{n} + \lambda \tag{1}$$

here, Re_{pore} $[= \rho v_0 d_p/\mu(1-\varepsilon_{\text{bed}})]$ is the pore Reynolds number, f_{pore} is the friction factor. α, β and λ are the constants. Except Tallmadge (1970), the value of β is fixed at 0.

Darcy law deviates as fluid velocity increases, since inertial contribution starts dominating. Thus in order to account the solutions for the complete regime of flow,

* Tel.: +91 01302484085/+91 09419722212.
E-mail address: avdhesh_sharma35@yahoo.co.in

0142-727X/$ - see front matter © 2007 Elsevier Inc. All rights reserved.
doi:10.1016/j.ijheatfluidflow.2007.02.002

Nomenclature

A	area (m^2)
CV	control volume
d_p	current particle size (m)
k	thermal conductivity (W/m K)
m	mass flow rate (kg/s)
n_{Tuy}	number of tuyers
Q_{gen}	heat generation (kW)
T	temperature (K)
Y	mass fraction
A_m	mean area (m^2)
d	particle diameter (m)
D	geometrical diameters (m)
K	pressure drop parameter
m_{gm}	mean gas flow in each CV
ΔP	pressure drop (N/m^2)
R	gasifier tube radius (m)
T_A	ambient temperature (K)
T	thickness (m)
C_{1-4}	constants
d_b	initial particle diameter (m)
D_t	tube diameter (m)
l	length (m)
Δm_s	solid mass conversion
Q	heat (kW)
Re	Reynolds number
ΔT	temperature drop in unit cell
v_0	superficial velocity (m/s)

Greek letters

μ	viscosity ($kg\ m^{-1}\ s^{-1}$)
σ_{ex}	extinction coefficient
$\bar{\varepsilon}_{bed}$	average bed porosity
ρ	density (kg/m^3)
f	friction factor
θ	angle
$\langle\overline{\sigma_{ex}}\rangle$	scaled extinction coefficient
$\varepsilon_{bed}(r)$	radial bed porosity
Y_s	sphericity
λ	constant
σ	Stefan–Boltzmann constant
ε_{bed}	Bed porosity (bulk)
α, β	constants
ξ	correction factor at reactor wall

Subscripts/superscripts

A	ambient
bd	dry biomass
char	char
con	contact of particles
gen	generation/released (heat)
preheat	preheating zone
sg	solid–gas–fluid contact
Tuy	tuyer
oxd	oxidation
air	air
dry	drying zone
cl	unit cell
Dev	developing flow
pyr	pyrolysis
pg	producer gas
s, g	solid, gas
vol	volatile
red	reduction
ash	ash
eff	effective
ct	contact of two particles
Fd	fully developed flow
pore	pore
rad	radiation
Top	open top
w	water vapour

Forchheimer proposed the first expression in 1901, which is based on dimensional correlation (Churchill, 1988).

$$-\Delta P/l = \alpha^* \mu v_0 + \beta^* \rho v_0^2 (-\Delta P/1) \quad (1a)$$

where α^* and β^* are the constants. Ergun (1952) combined the Carman–Kozeny equation, and Blake–Plummer equation in form of Forchheimer equation. Macdonald (Churchill, 1988; Kaviany, 1995) successfully used the Forchheimer's equation and correlate data separately for different types of porous media in terms of various parameters including particle surface roughness. In order to implement these models to the chemical reactors/gasifiers, uncertainties still exist- (i) varying tube-to-particle diameter ratios and (ii) drag due to reactor wall. Various authors address these issues for packed bed (Mehta and Hawely (Churchill, 1988); Cohen and Metzner (1981); Winterberg and Tsotsas (2000a); Winterberg and Tsotsas (2000b).) Mehta and Hawely describe the wall drag by taking the surface area of the tube into account in the definition of the hydraulic diameter, while Winterberg and Tsotsas (2000a,b) handle the radial porosity variation and wall drag in packed tubes. Sharma et al. (2004) developed an interesting fluid analysis to relate air and gas flow through the porous bed of biomass gasifier, with increasing fluid flow and decreasing particle size in the direction of flow.

Extensive work has been carried out on heat transfer in packed bed (Singh and Kaviany, 1992; Cheng et al., 1999; Kikuchi, 2001; Sharma, 2006). These include many approaches. The approach using effective thermal conductivity, k_{eff}, of the packed bed has been most popular in the recent literature (Chen and Churchill, 1963; Kaviany,

1995; Slavin et al., 2002; Kamiuto and Yee, 2005; Sharma, 2003, 2005). Slavin et al. (2002) have used the measurable parameter, surface roughness of the particle to avoid the use of any adjustable parameters in the determination of k_{eff} for uniform metallic spheroids filled with ideal gas with no compression of particles. Sharma (2003) considered a packed bed of biomass and char filled with gas mixture, with surface contact between particles due to compression, Sharma (2005) further extended the k_{eff} model for radiation transport by modifying shape factor using the extinction coefficient and also developed the heat transfer model using single control volume applied to the bed of gasifier.

Logtenberg et al. (1999) have reported a fluid flow and heat transfer CFD model using 3-D Navier–Stocks equations. Marafie and Vafai (2001) reported a non-thermal equilibrium, two-equation model to represent the fluid transport and energy transport. Jamialahmadi et al. (2005) presented a mathematical model for the prediction of pressure drop, bubble size, gas hold up and heat transfer accurately.

In the present contribution, the focus is on analysis of heat transfer and fluid flow considering axial, radial variation in bed porosity along with the effect of wall drag in order to predict accurate various flow rates, pressure drop, temperature profile through the gasifier bed and apportionment of air inflow from open top to tuyers.

2. System description and experiments

The open top downdraft biomass gasifier of capacity 20 kWe developed in Indian Institute of Science, Bangalore (Sharan et al., 1997) marketed by NETPRO has been chosen for the present work (Fig. 1). In this design, air enters from top as well as from radial tuyers and the producer gas exits from the bottom of the reactor. The gas is than made to pass through an annulus around preheating zone so as to utilize a part of its heat for preheating of biomass. The outer wall of the gasifier is insulated to improve the thermal efficiency of the reactor. The system using producer gas for motive power generation, the gasifier should be coupled with a suitable cooling and cleaning unit. The blower has been used in the gas pipeline to create required suction to draw the gas.

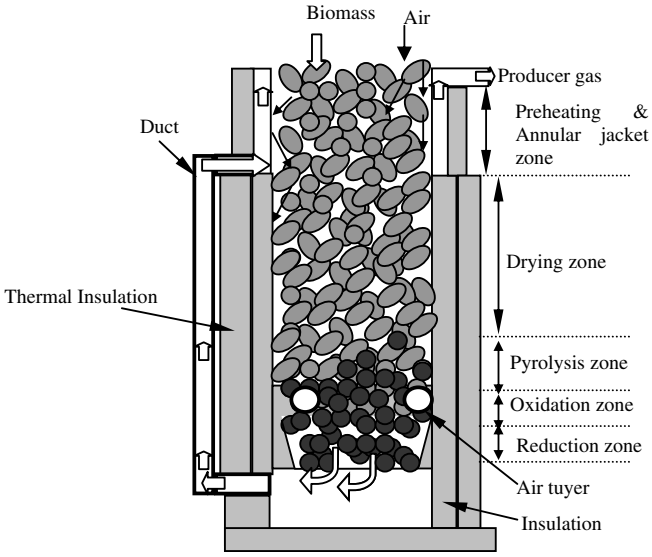

Fig. 1. Sectional view of IISc-DASAG gasifier.

In order to validate the model, the experimental data has been generated for IISc-DASAG gasifier. The gasifier was ignited and time was allowed (about 20 min) for the initial transients to subside. Then the temperatures at various locations inside the reactor were recorded using calibrated K-type (Chromel-alumel) thermocouples. Two single-channel digital temperature indicators, a 12-channel selector switch were used in the present work to read out the temperature values at various locations. The pressure at tappings P1 is recorded using U-tube manometer arrangements. Flow rate of producer gas was measured using a calibrated venturi meter. The procedure was repeated for different gas flow rates. The experimental set-up of a gasifier system has been shown schematically in Fig. 2.

3. Formulation

The packed bed in the gasifier has been modeled as a saturated porous medium in which fluid flow increases in the direction of flow due to gasification of the particles constituting the bed. The flow of air and biomass consumption in a biomass gasifier is closely coupled with thermo-chemical processes. For simplicity, the gasifier is divided into six zones, each one corresponding to a dominant phenomenon as: preheating, drying, pyrolysis, oxidation and reduction zones. The annular jacket is considered as a separate zone. The preheating, annular jacket zone and drying zones are further divided into 3 control volumes (CVs) each; and the pyrolysis zone is divided into 2 CVs. Oxidation and reduction zones are constituted by one control volume each.

3.1. Assumptions

The porous bed is assumed to be isotropic, where solid and gas is considered to be in thermal equilibrium. Within each zone, the particle size, bed porosity and temperature are assumed to be uniform. The following assumptions have been invoked for each zone:

Drying/preheating zone: The particles are taken to be spherical with equal diameters. Complete removal of moisture is assumed in this zone. No shrinkage in particle size.

Pyrolysis zone: All volatiles are assumed to be released in this zone and moving into gaseous phase leaving behind char and ash in the solid phase. Heat of the pyrolysis reactions is taken to be negligible.

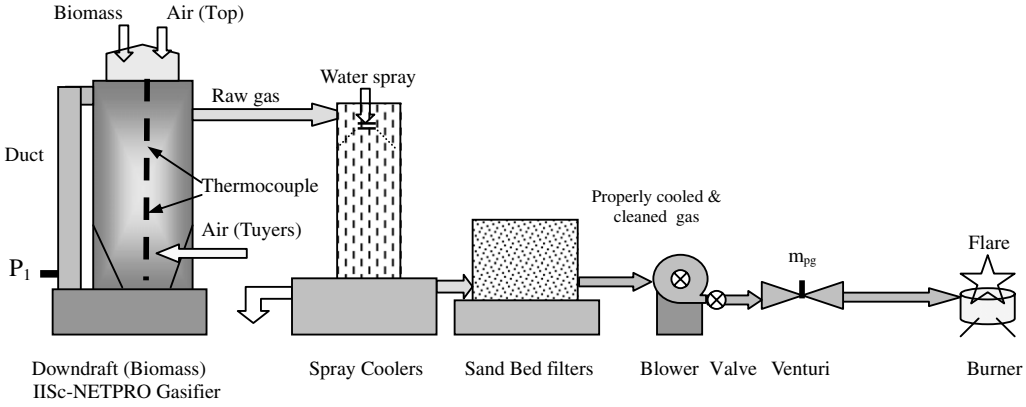

Fig. 2. Schematic diagram of a gasifier system.

Oxidation zone: Oxygen in available air is assumed to be completely consumed in this zone. Char oxidation is negligible in comparison with volatile oxidation.
Reduction zone: All char is taken to be consumed in this zone. The ratio of heat generation in oxidation zone to heat absorption in reduction zone is fixed at 2.8.

3.2. Mathematical equations

3.2.1. Mass balance

In the biomass gasifier, the consumption of biomass, water vapour, flow of air from open top and through the tuyers can be related with gas flow rate at the gasifier exit using global mass balance as

$$m_{\text{air}} = m_{\text{Top}} + n_{\text{Tuy}} m_{\text{Tuy}} = m_{\text{pg}} - m_{\text{bd}} - m_{\text{w}} - m_{\text{ash}} \tag{2}$$

During gasification process, the solid phase converts progressively into gaseous phase as a result of thermo-chemical reactions taking place in the chemically reactive bed of downdraft (biomass) gasifier. The local mass balance for each control volume in the fuel bed can be written as

$$(\Delta m_{\text{s}})_I = (m_{\text{s}})_{I-1} - (m_{\text{s}})_I = (m_{\text{g}})_I - (m_{\text{g}})_{I-1} \tag{3}$$

where solid phase (s) comprises of biomass, char and ash, while gaseous phase (g) comprises of water vapour, volatiles, air and product gas. The solid conversion Δm_{s} in drying and preheating zone is due to evaporation, thus, fraction of dry biomass, Y_{db}, and moisture content, Y_{w}, can be represented as

$$Y_{\text{db}} + Y_{\text{w}} = 1 \tag{4}$$

In the pyrolysis zone, the mass fractions Y of volatile, char and ash can be related as

$$Y_{\text{vol}}^{\text{pyr}} + Y_{\text{char}}^{\text{pyr}} + Y_{\text{ash}}^{\text{pyr}} = 1 \tag{5}$$

here, Y^{pyr} denotes the mass fractions in dry wood and its subscripts viz., vol, char and ash denote the volatile, char and ash respectively. The solid conversion during the pyrolysis process is obtained from the literature (Ragland and Aerts, 1991). During oxidation and reduction however the total char is consumed to form gases. Thus,

$$Y_{\text{char}}^{\text{oxd}} + Y_{\text{char}}^{\text{red}} = 1 \tag{6}$$

here, $Y_{\text{char}}^{\text{oxd}}$ and $Y_{\text{char}}^{\text{red}}$ are the fractions of char consumed in the oxidation and reduction zones respectively.

3.2.2. Momentum balance

While the Darcy's law for flow through different types of porous media is valid for $Re_{\text{Dp}} \leqslant 1$, when $Re_{\text{Dp}} > 1$, the inertial effects needs to be accounted for in the momentum balance. Thus, the correlations of Ergun (1952) and Macdonald (Kaviany, 1995) as given in Table 1 are used in the present work for comparative analysis of the pressure drop through granular bed of gasifier.

In Table 1, K_{perm} is the permeability of the medium, l is the thickness of bed, v_0 ($= m/(A\rho)$) is the superficial velocity and Re_{Dp} ($= \rho v_0 d_{\text{p}}/\mu$) is the Reynolds number for particle. The general equation to predict the pressure drop through the Ith CV in gasifier bed in terms of average fluid

Table 1
Correlations for prediction of pressure drop in porous bed

S. no.	Correlations	Reference
I	$-\frac{\Delta P}{l} = \alpha_{\text{E}}\mu v_0 \frac{(1-\varepsilon_{\text{bed}})^2}{\varepsilon_{\text{bed}}^3 d_{\text{p}}^2} + \beta_{\text{E}}\rho v_0^2 \frac{(1-\varepsilon_{\text{bed}})}{\varepsilon_{\text{bed}}^3 d_{\text{p}}}$	Ergun (1952) [$\alpha = 150$; $\beta = 1.75$]
II	$-\frac{\Delta P}{l} = \alpha_{\text{M}}\rho v_0^2 \frac{(1-\varepsilon_{\text{bed}})^2}{Re_{\text{Dp}}\varepsilon_{\text{bed}}^3 d_{\text{p}}} + \beta_{\text{M}}\rho v_0^2 \frac{(1-\varepsilon_{\text{bed}})}{\varepsilon_{\text{bed}}^3 d_{\text{p}}}$	Macdonald (Kaviany, 1995) [$\alpha = 180$; $\beta = 1.8$–4.0]

flow rate (m_{gm}), particle size and fluid density may be expressed as

$$\Delta P_I = \left(\frac{\alpha(1-\bar{\varepsilon}_{bed})^2\mu(T_I)l_I}{\Psi_s^2\rho(T_I)\bar{\varepsilon}_{bed}^3 A_m}(\xi/d_p)^2\right)m_{gm} + \left(\frac{\beta(1-\bar{\varepsilon}_{bed})l_I}{\Psi_s\rho(T_I).\bar{\varepsilon}_{bed}^3 A_m^2}(\xi/d_p)\right)m_{gm}^2 \quad (7)$$

here, α and β are the two constants the values of which are given in Table 1. Macdonald fixed β at 1.8 for smooth surface while 4 for rough surface. Ψ_s is the particles sphericity, A_m is the average cross-sectional area of gasifier tube in each CV. In Eq. (7), the Mehta and Hawely (Churchill, 1988) proposed the correction factor ξ to compensate the drag of the confining wall by introducing surface area of the wall.

$$\xi = [1 + (2/3)(d_p/D_t)/(1-\varepsilon_{bed})] \quad (7a)$$

Around the periphery of oxidation zone of the IISc-NET-PRO gasifier, the three tuyers are radially distributed at an angle of 120° to supply the air for gasification as shown in Fig. 3. These tuyers are made of straight pipe. The pressure drop across a tuyer is modeled as the developing regime for nearly the range of under consideration as given by

$$\Delta P_{Tuy} = \left(\frac{K_{Tuy} + f_{Tuy}L_{Tuy}/D_{Tuy}}{2\rho_{air}A_{Tuy}^2}\right)m_{Tuy}^2 \quad (8)$$

here, K_{Tuy} is the pressure loss parameter to represent the combined effect of entrance and exit for the tuyer.

In laminar fully developed flow ($Re < 2300$), Darcy–Weisbach friction-factor, f_{fd} is $64/Re$ while for turbulent flow, Blasius' relation gives, $f_{fd} = 0.316/Re^{0.25}$ for $Re < 10^5$ (Fox and McDonald, 1995). The developing length for laminar flow is given by $L_{Dev} \cong 0.06\ Re\ D_{Tuy}$, while for turbulent flow $L_{Dev} \cong 4.4ReD_{Tuy}^{1/4}$. Average pressure drop parameter from entrance to asymptotic region of fully developed flow denoted by K_{Dev} is given by the following relation obtained by curve fitting to the data of Schmidt and Zeldin (White, 1991) for laminar pipe flow

$$K_{Dev} = \exp\left(0.3 - 2.9\times10^{-3}\Big/\left(\frac{L_{Dev}}{ReD_{Tuy}}\right) - 1.43\times10^{-6}\Big/\left(\frac{L_{Dev}}{ReD_{Tuy}}\right)^2\right) \quad (9)$$

The Darcy friction factor for the developing region is then modified as

$$f_{Tuy} = f_{fd} + \frac{K_{Dev}}{L_{Tuy}/D_{Tuy}} \quad (10)$$

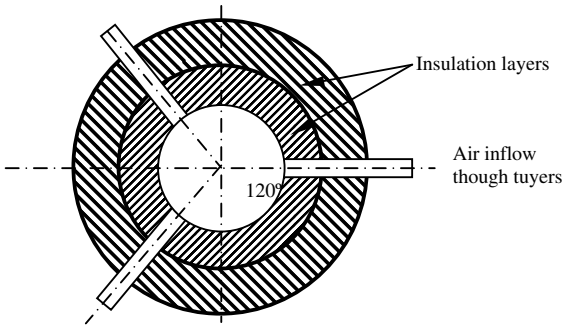

Fig. 3. Top view of the gasifier.

3.2.3. Energy balance

The axial and radial heat transport in gasifier bed accounted for advective, conductive and radiative heat fluxes at the boundaries of each control volume in the porous bed. The axial heat transfer accounted for thermal interactions between the neighboring CVs, while the radial heat loss is describing the heat loss to the surroundings. The advection is due to the flow of gas as well as biomass/char down the bed of the gasifier as depicted in Fig. 4. Thus, for each CV of each zone, the energy equation is written as

$$[m_s h_s + m_g h_g]_{I-1} + Q_{diff,I-1} + Q_{gen,I} - Q_{loss,I} = [m_s h_s + m_g h_g]_I + Q_{diff,I} \quad (11)$$

here $h = \int Cp\,dT$, is the sensible enthalpy change with respect to surroundings, it comprises of solid phase (biomass, char and ash) and gaseous phase (water vapour, volatiles, air and combustion products).

Heat loss to the surroundings, Q_{loss}, is modeled in terms of equivalent thermal resistance, R_s, as

$$Q_{loss,I} = \frac{T_I - T_A}{R_{s,I}} = \frac{T_I - T_A}{R_{t(ins,I)} + R_{t(air,I)}} \quad (12)$$

Here $R_{t(ins,I)}$ and $R_{t(air,I)}$ are the resistance due to insulation at wall and outer surface of Ith CV in the bed. $Q_{diff,I-1}$ and $Q_{diff,I}$ denote the heat blast in and out, and are modeled as

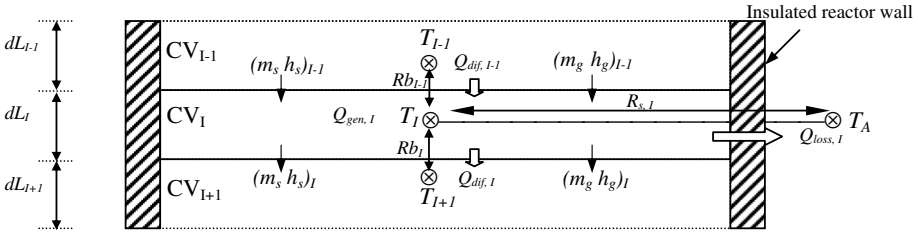

Fig. 4. Energy balance for the control volume.

$$Q_{\mathrm{diff},I-1} = (-k_{\mathrm{eff}} A \nabla T)_{I-1} = \frac{T_{I-1} - T_I}{R_{\mathrm{b},I-1}};$$
$$Q_{\mathrm{diff},I} = \frac{T_I - T_{I+1}}{R_{\mathrm{b},I}} \tag{13}$$

$R_{\mathrm{b},I}$ and $R_{\mathrm{b},I-1}$ are the thermal resistances in axial direction due to thermal interaction of CV_I with upper CV_{I-1} and lower CV_{I+1}. Q_{gen} denotes the heat generation and depends on the process in a control volume: drying results in absorption of latent heat of vaporization, pyrolysis results in heat of pyrolysis, oxidation or reduction processes results the heat generation or absorption due to gasification process.

3.2.4. Effective thermal conductivity

The sub-model of effective thermal conductivity, schematically represented in Fig. 5 has been described here for clarity.

The contribution of conduction transport in the effective thermal conductivity follows the model of Sharma (2005), while contribution of radiation transport k_{rad} has been adapted from the model of Sharma (2006). Here a cylindrical unit cell consists of two half spherical particles contacting each other with θ_{ct} as the half angle of contact. Heat transfer is assumed to be in the vertical direction parallel to the axis connecting the two spheres. Two conductive paths are considered between the two – the central region of the width of the contact surface, and the surrounding region where the heat transfer passage is from solid particle to the fluid in the void and then again through the solid particle, while the third path describes the radiation transport between the bed particles. For the model formulation, the particles are assumed to be spherical with equal diameter. The overall temperature drop, ΔT, in the cylindrical unit cell given as

$$\Delta T = \Delta T_{\mathrm{s}} + \Delta T_{\mathrm{g}} + \Delta T'_{\mathrm{s}} \tag{14}$$

The heat conduction through solid–fluid–solid region in the unit cell can be represented by

$$k_{\mathrm{s}} \Delta T_{\mathrm{s}} \int_{\theta_{\mathrm{ct}}}^{\frac{\pi}{2}} \frac{2\pi r\,\mathrm{d}r}{(d_{\mathrm{p}}/2)\cos\theta} = k_{\mathrm{g}} \Delta T_{\mathrm{g}} \int_{\theta_{\mathrm{ct}}}^{\frac{\pi}{2}} \frac{2\pi r\,\mathrm{d}r}{d_{\mathrm{p}}(1-\cos\theta)} = \frac{k_{\mathrm{eff,sg}} A_{\mathrm{cl}} \Delta T}{l_{\mathrm{cl}}} \tag{15}$$

here, $k_{\mathrm{eff,sg}}$ represents the contribution of conduction in solid–fluid–solid region to the effective thermal conductivity; A_{cl} is the cross-sectional area of the unit cell and l_{cl} is its length, with $A_{\mathrm{cl}} = \pi d_{\mathrm{p}}^2/4$; $l_{\mathrm{cl}} = d_{\mathrm{p}}$ and $r = (d_{\mathrm{p}}/2)\mathrm{Sin}\theta$. Integrating Eq. (15) for limit, $\theta = \theta_{\mathrm{ct}}$ to $\theta_{\max} = \pi/2$ and assuming d_{p} is constant within a unit cell $k_{\mathrm{eff,sg}}$ is given by

$$k_{\mathrm{eff,sg}} = \frac{2k_{\mathrm{s}}k_{\mathrm{f}}C_1(\ln C_2 + C_1)}{k_{\mathrm{g}}(\ln C_2 + C_1) - k_{\mathrm{s}}C_1} \tag{16}$$

where $C_1 = \mathrm{Cos}\,\theta_{\mathrm{ct}}$; $C_2 = 1 - \mathrm{Cos}\,\theta_{\mathrm{ct}}$; while θ_{ct} is based on particle contact following Enoeda (Slavin et al., 2002) who took the contact radii to be typically 0.7% of particle diameter. Similarly, determining the conduction through the contact region, $k_{\mathrm{eff,con}}$ is given by

$$k_{\mathrm{eff,con}} = \frac{k_{\mathrm{s}} d_{\mathrm{ct}}^2}{d_{\mathrm{p}}^2} \tag{17}$$

According to Sharma (2006), the contribution of radiation in the cylindrical unit cell can be modeled assuming the wavelength-independent properties and for $\Delta T < 200$ K, Tein and Drolen (1978) described the radiant conductivity assuming one-dimensional, plane geometry with emitting particles in steady state, a deep bed with zero reflectivity at wall. Thus

$$k_{\mathrm{eff,\,rad}} = \frac{16\sigma T^3}{3\langle\sigma_{\mathrm{ex}}\rangle} = 4\sigma\Omega d_{\mathrm{p}} T^3 \tag{18}$$

where Ω is the shape factor and can be calculated in terms of extinction coefficient, $\langle\sigma_{\mathrm{ex}}\rangle$. Kamiuto and Yee (2005) proposed the scaled extinction coefficient, $\langle\overline{\sigma_{\mathrm{ex}}}\rangle$ for large opaque particles as

$$\langle\overline{\sigma_{\mathrm{ex}}}\rangle = \left(1 - \frac{1}{2\gamma}\right)\langle\sigma_{\mathrm{ex}}\rangle = \frac{1.5(2\gamma-1)(1-\varepsilon_{\mathrm{bed}})}{d_{\mathrm{p}}} \tag{19}$$

$$\gamma = 1 + 1.5(1-\varepsilon_{\mathrm{bed}}) - 0.75(1-\varepsilon_{\mathrm{bed}})^2 \qquad \text{for } \varepsilon_{\mathrm{bed}} < 0.921 \tag{20}$$

For optically thick packed beds the internal radiant conductivity can be treated as a diffusive process. Thus, the effective thermal conductivity, k_{eff}, can be written as

$$k_{\mathrm{eff}} = k_{\mathrm{eff,sg}} + k_{\mathrm{eff,con}} + k_{\mathrm{eff,rad}} \tag{21}$$

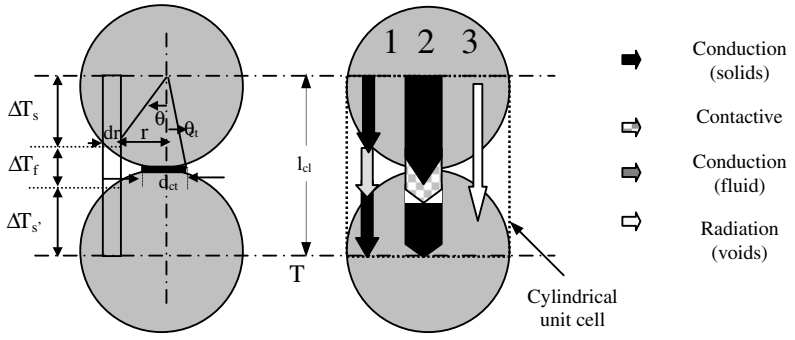

Fig. 5. Model of two contacting solid particles in the unit cell.

3.2.5. Particle size variation

Here the initial diameter of biomass (d_b) is an input parameter. In drying and preheating zones, there is no change in the diameter. However in pyrolysis, oxidation and reduction zones, feedstock undergoes chemical reactions leading to change in the particle size. As wood converts into char due to pyrolysis, its size reduces and its diameter at exit of pyrolysis zone can be given by

$$d_{\text{char}}^{\text{pyr}} = d_b(Y_{\text{char}}^{\text{pyr}}\rho_b/\rho_{\text{char}})^{1/3} \tag{22}$$

In oxidation zone, char is consumed to form gases. Particle size of char at the exit of this zone is given by

$$d_{\text{char}}^{\text{oxd}} = d_{\text{char}}^{\text{pyr}}[(1 - Y_{\text{char}}^{\text{oxd}})]^{1/3} \tag{23}$$

where ρ_b and ρ_{char} are the densities of the dry biomass particle and the char particle respectively. In the reduction zone, all char is consumed and only ash particles (1 mm diameter size) leave the reduction zone.

3.2.6. Bed porosity variation

Bulk porosity of bed, ε_{bed} is determined using the correlation suggested by Chen and Gunkel (1987)

$$\varepsilon_{\text{bed}} = 0.5 - 0.2\left(1 - \frac{d_p}{d_b}\right) \tag{24a}$$

Here d_p is the particle diameter in the current control volume.

Winterberg and Tsotsas, (2000) suggested the correlation for variation in radial porosity for spherical particles bed as

$$\varepsilon_{\text{bed}}(r) = \varepsilon_{\text{bed}}\left(1 + C_3 e^{-C_4\frac{R-r}{d_b}}\right) \tag{24b}$$

where $C_3 = 0.65/\varepsilon_{\text{bed}} - 1$, $C_4 = 6.0$

The averaged bed porosity $\bar{\varepsilon}_{\text{bed}}$ can be obtained by integration

$$\bar{\varepsilon}_{\text{bed}} = \frac{2}{R^2}\int_0^R \varepsilon_{\text{bed}}(r) r\,dr \tag{24c}$$

4. Solution procedure

The producer gas flow rate, air–fuel ratio and heat generation in oxidation zone are required as input to the model. Then biomass consumption rate, water vapour and air inflow from open top as well as through the tuyers can be related each other using the energy balance Eq. (11) and momentum balance Eq. (7) for pressure drop in bed and Eq. (8) for pressure drop through the tuyers are coupled with global mass balance Eq. (2) and local mass balance Eq. (3). Thus the sum of pressure drop across preheating, drying and pyrolysis zones can be related to pressure drop across the tuyers as

$$\Delta P_{\text{preheat}} + \Delta P_{\text{dry}} + \Delta P_{\text{pyro}} = \Delta P_{\text{Tuy}} \tag{25}$$

here subscripts preheat, dry and pyro denote the preheating, drying and pyrolysis zone respectively. The set of these equations for each 13 control volumes in conjunction with Eq. (25) is solved using Gauss–Siedel iteration of convergence to predict bed temperature profile and pressure drop across the gasifier bed. The total pressure drop across the gasifier thus is obtained as

$$\Delta P_g = \Delta P_{\text{preheat}} + \Delta P_{\text{dry}} + \Delta P_{\text{pyro}} + \Delta P_{\text{oxd}} + \Delta P_{\text{red}} \tag{26}$$

Here subscripts oxd and red denote the oxidation and reduction zone respectively.

5. Property data

The viscosity of gaseous phase is obtained from the correlation of Hagge and Bryden (2002) as given by

$$\mu(T) = 4.847 \times 10^{-7} T^{0.64487} \quad (\text{kg m}^{-1}\,\text{s}^{-1}) \tag{27}$$

Ragland and Aerts (1991) reported the thermal conductivity (W/m K) of char and biomass as given by

$$k_{\text{char}} = 0.67 S_{\text{char}} - 0.071$$

$$k_b = S_b(0.1941 + 0.4064 Y_w) + 0.1864 + 0.002(T - T_A) \tag{28a}$$

$$k_g \cong k_{\text{air}} = 3.0 \times 10^{-4} T^{0.79} \tag{28b}$$

here, S is the specific gravity (kJ/kg K) and its subscripts denote the biomass and char. Their values are obtained from literature (Ragland and Aerts, 1991). The data from Keenan et al. (Borman and Ragland, 1998) has been used to curve fit for thermal conductivity and specific heat of air and same curve fits are considered for gaseous phase, the relation is valid for $300 < T < 1500$ K.

The specific heat for working fluid (air) is obtained by curve fit to data of Keenan (Borman and Ragland, 1998)

$$Cp_{\text{bd}} = 0.1031 + 0.003867T$$

$$Cp_b = [Cp_{\text{bd}} + 4.19 Y_w]/(1 + Y_w) + 0.02355T - 1.32 Y_w - 6.2 Y_w \tag{29a}$$

$$Cp_{\text{char}} = 1.39 + 0.00036T$$

$$Cp_g \cong Cp_{\text{air}} = 0.931 + 0.0002T - 1.01 \times 10^{-8} T^2 \tag{29b}$$

However, the Cp_g and k_g values of product gas can be obtained from the gas composition.

Since the gaseous oxidation is very fast as compared to char oxidation (Ragland and Aerts, 1991) thus, the consumption of char in oxidation zone can be neglected in comparison with the char consumed in reduction zone ($Y_{\text{char}}^{\text{oxd}} \ll Y_{\text{char}}^{\text{red}}$).

6. Simulation results and discussion

The above model predicts the temperature profile, pressure drop through bed, airflow rates and apportionment of air inflow from the open top and through the tuyers for given mass flow rate of producer gas, air–fuel ratio, feedstock size and heat generation or absorption in each zone. Jayah et al. (2003) reported experimentally that the air–fuel ratio for gasification process does not vary much (1.9–2.3

for wide range of gas flow rates). Thus, in the present work, the air–fuel ratio is maintained at 2.3. A realistic model requires the complete kinetics and energetics of the pyrolysis, oxidation and reduction zones to be solved. The scope of this paper does not include these models. In order to account for actual hot flow conditions; the heat of pyrolysis, heat generation in oxidation zone and heat absorbed in reduction zone of the downdraft biomass gasifier are supplied as input parameters to the fluid flow and heat transfer model. For the present work, however, the overall pyrolysis is considered to be thermally neutral (Ragland and Aerts, 1991) and the ratio of Q_{oxd} and Q_{red} is fixed at 2.8 (Sheng, 1989). Using these approximations, the only parameter Q_{oxd} would be needed as input information to describe the overall chemistry of chemical reactions in the gasifier.

6.1. Validation

It is quite difficult to quantify the parameter Q_{oxd} from the traditional experiments on the gasifier. Thus, in order to validate the above fluid flow and heat transport model, the temperature profile may be supplied as input information to compare the predictions for the pressure drop through the gasifier bed against experimental data. The experiments are performed to obtain the temperature profiles and gasifier pressure drops through the gasifier bed at different gas flow rate (described in Section 2: System description and experiments). These temperature profiles are converted into zonal temperature specifications for various flow rates as listed in Table 2. The height of preheating, drying, pyrolysis, oxidation and reduction zone are taken as 100, 60, 7, 17 and 17 cm respectively.

With these temperatures specifications of each zone at the corresponding gas flow rates (Table 2), zone heights, with varying particle size distribution (Eqs. (22) and (23)); the simulations are performed for typical particle size of 38 ± 2 mm. The model predictions for pressure drop through bed in hot flow conditions are compared with experimental data as shown in the Fig. 6. The good agreement between predictions for pressure drop and experiments for actual operating condition is obtained. As expected, the pressure drop is found to be increased with increasing gas flow rates.

6.2. Parametric analysis

After validation of the model, the parametric analysis has been carried out to investigate the effect of parameters

Table 2
Zonal temperature specifications obtained from experiments

m_{pg} (g/s)	$T_{preheat}$	T_{drying}	T_{pyr}	T_{oxd}	T_{red}
10.6	301	303	880	1270	945
8.5	301	303	870	1207	940
6	301	303	860	1204	930
4.7	301	304	840	1150	920

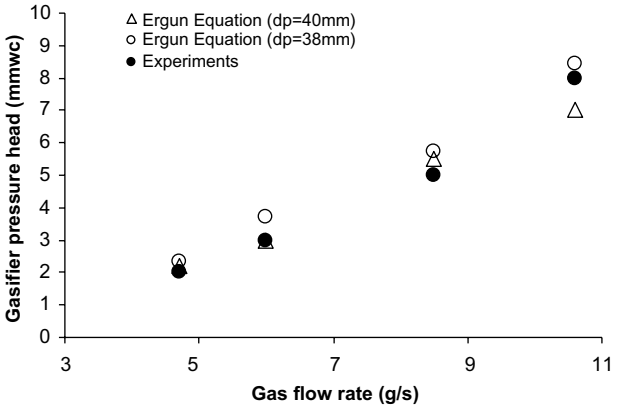

Fig. 6. Comparing the predictions of gasifier pressure drop with measurements for various gas flow rate, $Y_w = 0.11$, $\Phi = 0.4$, Ergun correlation.

on the temperature profile and pressure drop through the gasifier bed. The baseline values for heat generation in oxidation zone, Q_{oxd}; gas flow rate at exit, m_{pg}, and air–fuel ratio are fixed at 11.0 kW, 8 g/s, 2.3, respectively. With these baseline values and for spatially varying particle size distribution for d_b value of 3 cm, the simulations are performed to investigate the effects of parameters – effective thermal conductivity, gas flow rate, heat released in oxidation zone, moisture content, particle size, air inlet temperature and thickness of insulation at reactor wall on the temperature profile and pressure drop through the gasifier bed.

6.2.1. Effective thermal conductivity

The predictions of temperature profile using the effective thermal conductivity model described in the present work have been compared with Petersen et al. (1997) and Slavin et al. (2002) as shown in Fig. 7, while Fig. 8 shows the predictions for gasifier pressure drop through gasifier bed. The graphs reveal that the case with higher temperature profile in the gasifier bed predicts slightly higher value of pressure drop. At higher temperature the density of gases is lower,

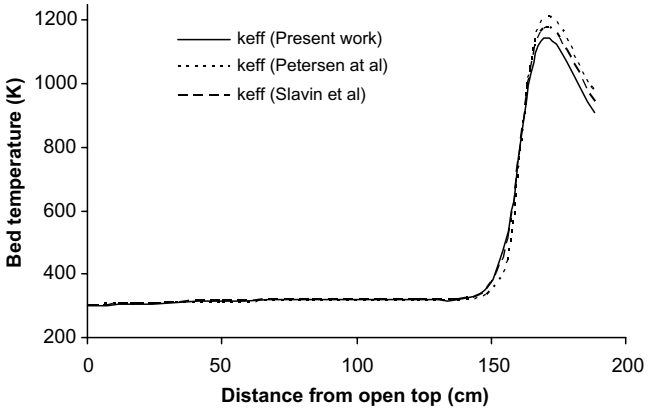

Fig. 7. Effect of k_{eff} on bed temperature profile, $m_{pg} = 8$ g/s, $Q_{oxd} = 11$ kW, $d_b = 3$ cm.

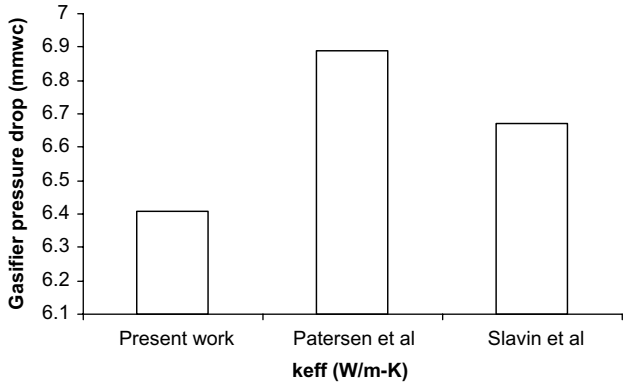

Fig. 8. Effect of k_{eff} on the pressure drop, $m_{pg} = 8$ g/s, $Q_{oxd} = 11$ kW, $d_b = 3$ cm, Ergun correlation.

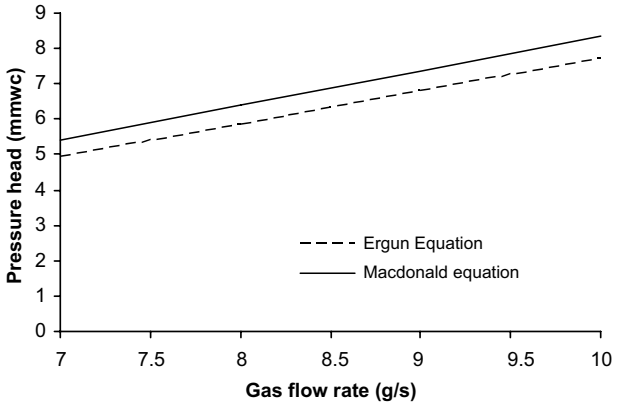

Fig. 10. Effect of gas flow rate at gasifier exit, m_{pg}, $Q_{oxd} = 11$ kW, $d_b = 3$ cm.

resulting in slightly higher velocities for given gas flow rate. Increased velocity and viscosity due to rise in temperatures, results in relatively higher pressure drop. If the temperature is doubled in a given CV, the fluid density is halved resulting in doubling of the fluid velocities, for a given mass flow rate of gas. Since there is a quadratic dependence of pressure drop on velocity (Table 1), the corresponding increase in pressure drop in a given control volume will be nearly fourfold. Similarly the dependence of gas viscosity follows power law with temperature as given by the Eq. (27).

6.2.2. Gas flow rate

The effect of variation in gas flow rate from 7 to 10 g/s has been studied on the bed temperature profile and pressure drop through the bed for given heat generation in oxidation is shown in Figs. 9 and 10. Figs. 9 shows that the temperature of pyrolysis, oxidation and reduction zones decreases with increasing the gas flow rate due to greater advection of heat away from these zones. As expected, the pressure drop will be higher at high flow rate, since it offers higher resistance to flow due to increased velocity through the pores. Predictions for pressure drop also show that Macdonald equation for porous bed gives slightly higher values of pressure drop as compared to Ergun equation.

6.2.3. Heat generation in oxidation zone

The effect of variation in heat generation in oxidation zone from 10 to 12 kW has been plotted against the temperature and pressure drop scale as shown in Figs. 11 and 12. Fig. 11 shows that the temperature of the bed increases significantly with increase in heat generation in oxidation zone. An increase of 54 °C in oxidation zone temperature has been observed for increasing the heat generation in oxidation zone from 10 to 11 kW at typical gas flow rate of 8 g/s. As expected, increasing the heat generation in oxidation zone results higher temperature of the neighboring zones (downstream reduction zone and/or upstream pyrolysis zone), while the temperatures in the drying and preheating zones do not show any significant effect. Fig. 12, shows that the pressure drop across the gasifier bed increases marginally with increase in heat generation in oxidation zone. As the temperatures in oxidation and reduction zones improve significantly with heat generation in oxidation zone, leading to increase in pressure drop through the gasifier bed.

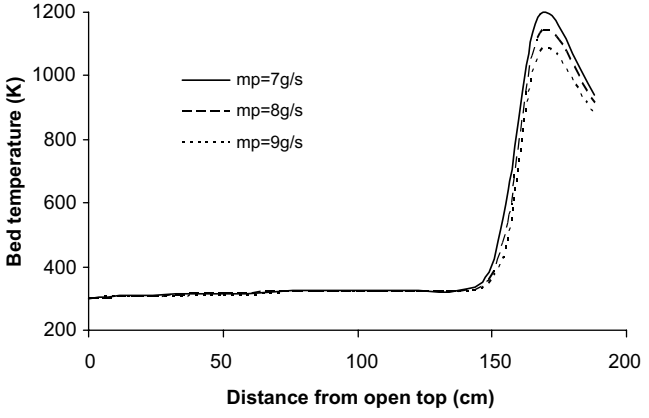

Fig. 9. Effect of gas flow rate at gasifier exit, m_{pg}, $Q_{oxd} = 11$ kW, $d_b = 3$ cm.

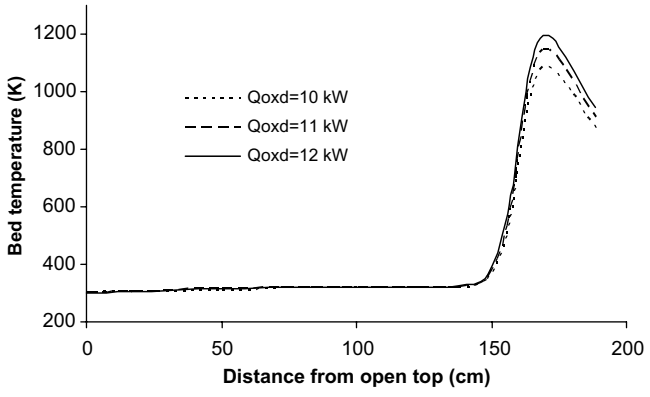

Fig. 11. Effect of heat generation in oxidation zone, $m_{pg} = 8$ g/s, $d_b = 3$ cm.

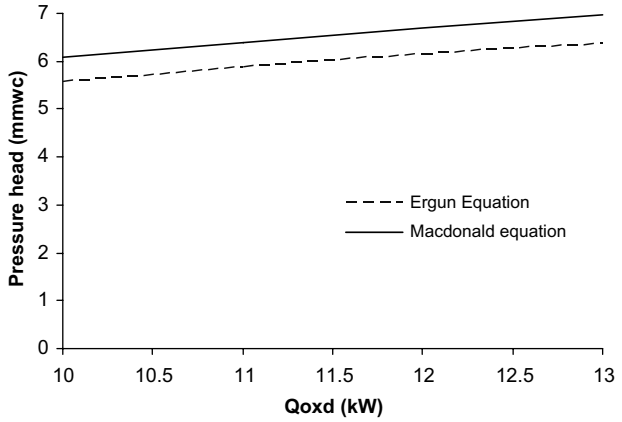

Fig. 12. Effect of heat generation in oxidation $m_{pg} = 8$ g/s, $d_b = 3$ cm.

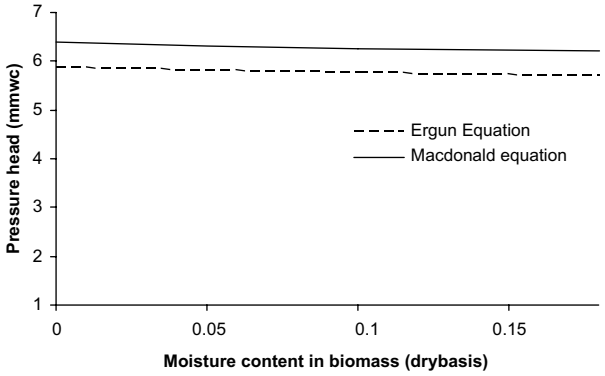

Fig. 14. Effect of moisture content in biomass, $m_{pg} = 8$ g/s, $Q_{oxd} = 11$ kW, $d_b = 3$ cm.

6.2.4. Moisture content

The moisture content in biomass feedstock is a critical operating parameter and the success of gasification operation depends on it. The moisture content of sun dried wood used as biomass feedstock varies up to 20% dry basis (Ragland and Aerts, 1991). The effect of variation of moisture content in dry biomass on the bed temperature and pressure drop is shown in Figs. 13 and 14. As moisture content in dry biomass increases, the temperature near the drying zone decreases (5). It could be expected due to the evaporation and superheating of the water vapour, while the temperatures of oxidation and reduction zone do not show any significant effect with variation in moisture content in feedstock. Fig. 14 does not show any significant effect of moisture content on the pressure drop, since the variation of temperature in oxidation and reduction zone is insignificant (5).

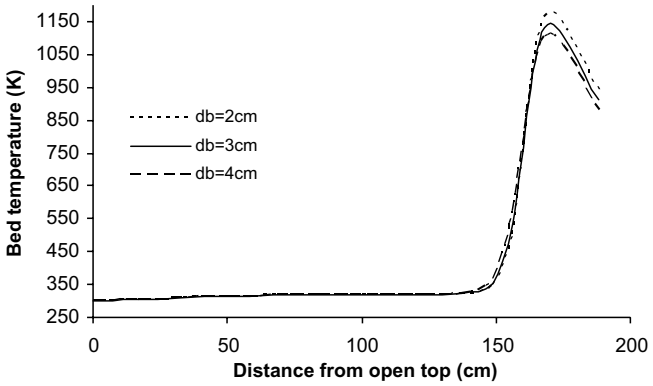

Fig. 15. Effect of feedstock diameter, d_b, on $m_{pg} = 8$ g/s, $Q_{oxd} = 11$ kW.

6.2.5. Particle size

The variation of initial feedstock size from 2 to 4 cm has been investigated on bed temperature profile and pressure drop through gasifier bed for spatially varying particle size distribution as shown in Figs. 15 and 16. Fig. 15 shows that the temperatures in oxidation and reduction zone improve

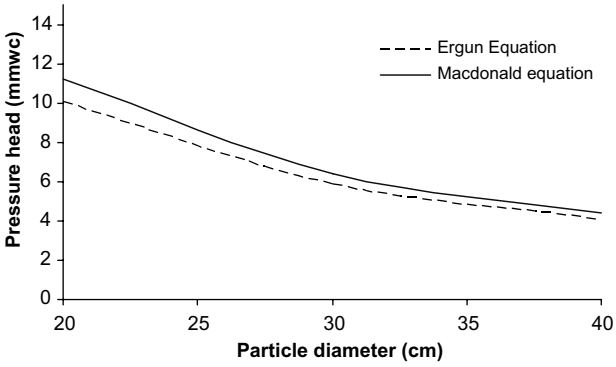

Fig. 16. Effect of feedstock diameter, d_b, on $m_{pg} = 8$ g/s, $Q_{oxd} = 11$ kW.

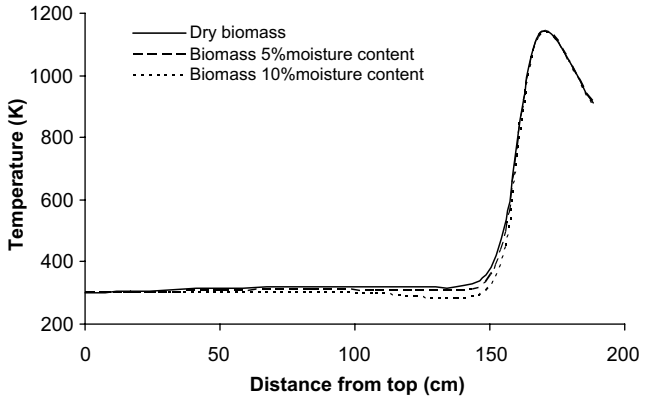

Fig. 13. Effect of moisture content in biomass $m_{pg} = 8$ g/s, $Q_{oxd} = 11$ kW, $d_b = 3$ cm.

significantly with reduction in feedstock size. The pressure drop in the bed decreases considerably with increase in particle size (16). The effect of variation in particle size on temperature is understandable, since the contribution of radiation in the effective thermal conductivity of the bed increases with increase in particle size (Eq. (18)), thus, the heat blast from the oxidation zone to the neighboring zones (i.e. pyrolysis and reduction zone) increases as particle size increases since the heat generation in oxidation zone is independent of particle size, therefore, the temperature of oxidation zone start decreasing with increase in particle

size. The pressure drop in the gasifier bed also decreases, since the pore size increases with particle size and thus offers less resistance to flow with increase in particle size of feedstock.

6.2.6. Input air temperature

Jayah et al. (2003) demonstrated that the hot air improves the gasifier performance, as it affects the air–fuel ratio for the gasification operation. The effect of preheating the input air from 300 to 400 K has been investigated here as shown in Figs. 17 and 18. Fig. 17 shows that the temperature profile improves considerably with rise in temperature of input air. The maximum temperature in the bed improves from 1133 to 1211 K for typical increase in air input temperature from 300 K to 400 K. Figs. 18 shows that pressure drop across the gasifier increases marginally with increase in input air temperature. Although the present gasifier design has been installed an annular jacket zone to recover the heat from the producer gas leaving the gasifier, yet the gas temperature even then is considerably high. The graph reveals that the length of heat recovery zone/annular jacket zone may be increased up to the pyrolysis zone in order to enhance the preheating of input air.

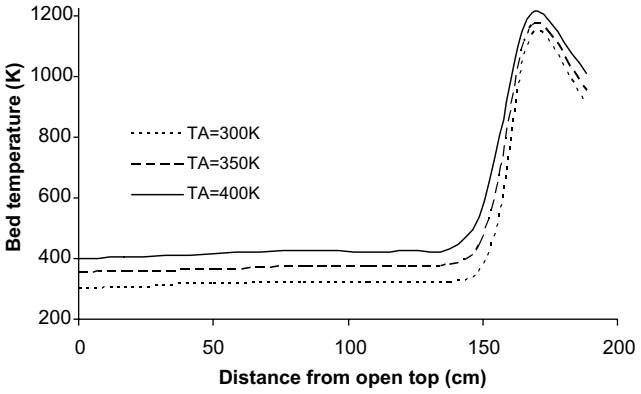

Fig. 17. Effect of ambient temperature, T_A, on $m_{pg} = 8$ g/s, $Q_{oxd} = 11$ kW, $d_b = 3$ cm.

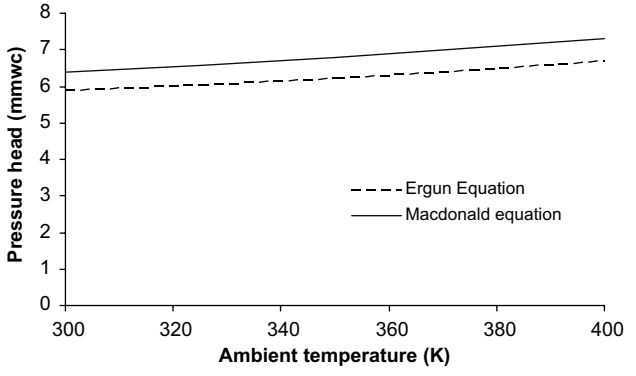

Fig. 18. Effect of ambient temperature, T_A, on the $m_{pg} = 8$ g/s, $Q_{oxd} = 11$ kW, $d_b = 3$ cm.

6.2.7. Thickness of thermal insulation

The lack of insulation thickness is the greatest contributor to heat loss, which also determines the thermal efficiency of the reactor. The effect on temperature profile and pressure drop in the gasifier bed is plotted in Figs. 19 and 20. As expected the temperature profile improves considerably with the initial increase in insulation thickness. An increase of about 47 °C in the temperature of oxidation and 73 °C in the reduction zone has been predicted for increasing the insulation of thickness at reactor wall from 2 cm to 30 cm at the typical gas flow rate of 8 g/s. Fig. 20 demonstrate the effect of insulation thickness on the pressure drop. The graph show the pressure drop increases sharply for initial increase in the insulation thickness thereafter it become almost independent of insulation thickness. For the present design, the insulation thickness should not be less than 15 cm, otherwise it may affect the pressure drop and the reaction temperatures in the bed and hence the performance of the reactor.

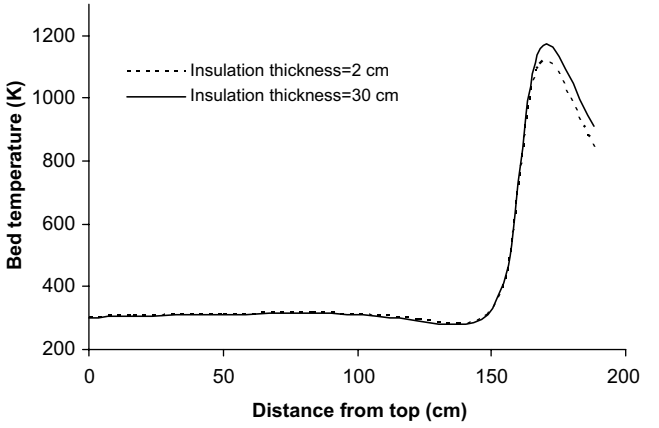

Fig. 19. Effect of insulation thickness on temperature profile $Q_{gen,4} = 11$ kW, $m_{pg} = 8$ g/s, $d_b = 3$ cm, $Y_w = 0.11$.

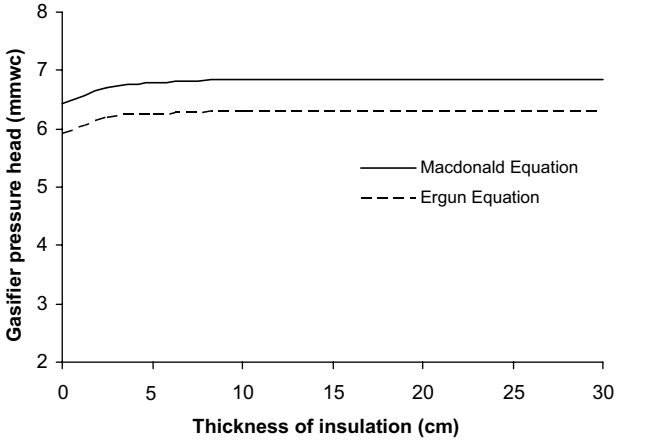

Fig. 20. Effect of insulation thickness on the pressure drop, $Q_{gen,4} = 11$ kW, $m_{pg} = 8$ g/s, $Y_w = 0.11$, $d_b = 3$ cm.

7. Conclusions

Fluid flow and heat transport model for the reactive, porous bed of biomass gasifier has been presented for simulating the apportionment of inflow air from open top and through tyurs, bed temperature profile, pressure drop through the gasifier bed. The conservation, fluid and heat transport model equations for biomass gasifier have been written for the six zones viz, preheating, annular jacket, drying, pyrolysis, oxidation and reduction zones; which comprises of total 13 CVs. Simulations are performed to predict the temperature profile and pressure drop for varying various operating parameters, viz., gas flow rate, heat generation in oxidation zone, moisture content in feedstock, particle size, and input air temperature. The simulated results show that the temperature profile is found to be very sensitive for gas flow rate, heat released in oxidation zone and input air temperature, while the temperature profile in the bed is found relatively insensitive for moisture content in feedstock.

The results also show that the high gas flow and bed temperature; and the reduction in feedstock size is found to cause a marked increase in pressure drop through the gasifier, while the pressure drop is relatively insensitive to the moisture content. The simulation also revealed that the size of heat exchanger may be extended up to the pyrolysis zone to enhance further preheating of the input air. The thickness of thermal insulation should not be less than 15 cm at reactor wall. The simulation shows that 40–50% of the total air induced is inducted through the three tuyers and the rest comes in through the open top. This ratio does not vary much with variation in temperature, producer gas flow rate or particle size.

Acknowledgement

The author likes to thank Dr. M.R. Ravi and Dr. S. Kohli at Dept. of Mechanical Engineering, Indian Institute of Technology, Delhi for helpful discussions and support.

References

Borman, G.L., Ragland, K.W., 1998. Combustion Engineering. McGraw-Hill International Ed., pp. 77–86.

Brownell, L.E., Gami, D.C., Miller, R.A., Nekarvis, W.F., 1956. Pressure drop through porous media. AIChE J. 9 (1), 79–81.

Chen, J.C., Churchill, S.W., 1963. Radiant heat transfer in packed beds. AIChE J. 9, 79–81.

Chen, J., Gunkel, W.W., 1987. Modeling & simulation of cocurrent moving bed gasification reactors–Part II. A detailed gasifier model. Biomass 14, 75–98.

Cheng, G.J., Yu, A.B., Zulli, P., 1999. Evaluation of effective thermal conductivity from the structure of a packed bed. Chem. Eng. Sci. 54, 4199–4209.

Churchill, S.W., 1988Viscous Flow – The Practical Use of Theory. Butterworth Publishers.

Cohen, Y., Metzner, A.B., 1981. Wall effects in laminar flow of fluids through packed beds. AIChE J. 27 (5), 705–715.

Comiti, J., Sabiri, N.E., Montillet, A., 2000. Experimental characterization of flow regimes in various porous media – III: Limit of Darcy's or creeping flow regime for Newtonian and purely viscous non-Newtonian fluids. Chem. Eng. Sci. 55, 3057–3061.

Ergun, S., 1952. Fluid flow through packed columns. Chem. Eng. Prog. 48, 89–105.

Fox, R.W., McDonald, A.T., 1995. Introduction to Fluid Mechanics, fourth ed. John Wiley & Sons Inc., Singapore.

Hagge, M.J., Bryden, K.M., 2002. Modeling the impact of shrinkage on the pyrolysis of dry biomass. Chem. Eng. Sci. 57, 2811–2823.

Jamialahmadi, M., Muller-Steinhagen, H., Izadpanah, M.R., 2005. Pressure drop. Gas hold-up and heat transfer during two phase flow through porous media. Int. J. Heat Fluid Flow 26, 156–172.

Jayah, T.H., Lu, Aye, Fuller, R.J., Stewart, D.F., 2003. Computer simulation of a downdraft wood gasifier for tea drying. Biomass Bioenergy 25, 459–469.

Kamiuto, K., Yee, S.S., 2005. Correlated radiative transfer through a packed bed of opaque spheres. Int. Commun. Heat Mass Transfer 32, 133–139.

Kaviany, M., 1995. Principles of Heat Transfer in Porous Media, second ed. Springer, New York.

Kikuchi, S., 2001. Numerical analysis model for thermal conductivities of packed beds with high solid-to-gas conductivity ratio. Int. J. Heat Mass Transfer 44, 1213–1221.

Logtenberg, S.A., Nijemeisland, M., Dixon, A.G., 1999. Computational fluid dynamics simulations of fluid flow and heat transfer at the wall-particle contact points in fixed-bed reactor. Chem. Eng. Sci. 54, 2433–2439.

Marafie, A., Vafai, 2001. Analysis of non-Darcian effects on temperature differentials in porous media. Int. J. Heat Mass Transfer 44, 4401–4411.

Petersen, S.B., Pedersen, L.Th., Henrisen, U., 1997. Theoretical and experimental investigation on heat transfer in fixed beds. In: Bridgewater, A.V., Boocock, D.G.B. (Eds.), Developments in Thermochemical Biomass Conversion, vol. 1. Blackie Academic and Professional, pp. 851–863.

Ragland, K.W., Aerts, D.J., 1991. Properties of wood for combustion analysis. Bioresource Technol. 37, 161–168.

Ranz, W.E., 1952. Friction and transfer coefficients for single particles and packed beds. Chem. Eng. Prog. 48, 247–253.

Sharma, Avdhesh Kr., 2003. New model of effective thermal conductivity in granular beds filled with gas. In: Proceedings of National Conference in Mechanical Engineering, 31st October and 1st November 03, vol. 1. organizing by MED, TIET, Patiala, India, p. 173–178.

Sharma Avdhesh Kr., 2005. IMECE2005-80758: Modeling conduction and radiation in the reactive, Porous bed of the gasifier. In: Proceedings of 2005 ASME International Mechanical Engineering Congress and Exposition, November 5–11, Orlando, Florida, USA.

Sharma, Avdhesh Kr., 2006. Modeling heat transfer in biomass gasifier. Paper code: HMT-2006-C184. In: Proceedings of 18th National and 7th ISHMT-ASME, Heat Transfer Conference, p. 315 (1315), IIT, Guwahati, India.

Sharan, H.N., Mukunda, H.S., Shrinivasa, U., Dasappa, S., 1997. IISc-DASANG biomass gasifiers: Development, Technology, Experience and economics. In: Bridgewater, A.K., Boocock, D.G.B. (Eds.), Development in Thermochemical Biomass Conversion, IEA Bioenergy, II, pp. 1058–1073.

Sharma, Avdhesh Kr., Kohli, S., Ravi, M.R., 2004. Modeling of fluid flow in a downdraft biomass gasifier. In: Proceedings of 2nd BSME-ASME International Conference on Thermal Engineering, January 2–4, 2004, vol. 2, BUET, Dhaka, pp. 861–866.

Sheng, G.X., 1989. Biomass gasifiers: from waste to energy production. Biomass, 3–12.

Singh, B.P., Kaviany, M., 1992. Modeling radiative heat transfer in packed beds. Int. J. Heat Mass Transfer 35, 1397–1405.

Slavin, A.J., Arcas, V., Greenhalgh, C.A., Irvine, E.R., Marshall, D.B., 2002. Int. J. Heat Mass Transfer 45, 4151.

Tallmadge, J.A., 1970. Packed bed pressure drop – an extension to higher Reynolds numbers. AIChE J. 16 (6), 1092–1093.

Tein, C.L., Drolen, B.L., 1978. Thermal Radiation in particulate media with dependent and independent scattering. A Rev. Numer. Fluid Mech. Heat Transfer 1, 1–32.

White, F.M., 1991. Viscous Fluid Flow. Mech. Engg. Series, third ed. MGH, Singapore.

Winterberg, M., Tsotsas, E., 2000a. Impact of tube-to-particle-diameter ratio on pressure drop in packed beds. AIChE J. 46 (5), 1084–1088.

Winterberg, M., Tsotsas, E., 2000b. Correlations for effective heat transport coefficients in beds packed with cylindrical particles. Chem. Eng. Sci. 55, 5937–5943.